physchem

Article

Critical Review of C_p Calculation Within the Fluidized Bed of Cement Rotary Kilns

Evanthia Kostarellou [1], Evdokia Gkagkari [1], Michail Mouratidis [1], Theodoros Damartzis [1,2], George Skevis [1], Alexandros Katsinos [3], Thomas Kaimakamis [3], Ananias Tomboulides [3], Vasileios K. Michalis [4], Vasileios Stroungaris [4], Nikolaos Poulianas [4], Marios S. Katsiotis [4], Akrivi Asimakopoulou [1] and Ioannis N. Tsimpanogiannis [1,*]

1 Laboratory of Advanced Renewable Technologies & Environmental Materials in Integrated Systems, Chemical Process & Energy Resources Institute, Centre for Research & Technology Hellas, 57001 Thermi, Greece; kevanthia@certh.gr (E.K.); evdokia.gkagkari@certh.gr (E.G.); michalis.mouratidis@certh.gr (M.M.); damartzis@cheng.auth.gr (T.D.); gskevis@certh.gr (G.S.); asimak@certh.gr (A.A.)
2 Laboratory of Chemical Process and Plant Design, Department of Chemical Engineering, Aristotle University of Thessaloniki, 54124 Thessaloniki, Greece
3 Laboratory of Applied Thermodynamics, Department of Mechanical Engineering, Aristotle University of Thessaloniki, Engineering Building D, University Campus, 54124 Thessaloniki, Greece; katsinos@auth.gr (A.K.); thomaskaimak@gmail.com (T.K.); ananiast@meng.auth.gr (A.T.)
4 TITAN Cement S.A., 11143 Athens, Greece; v.michalis@titancement.com (V.K.M.); v.stroungaris@titan.gr (V.S.); n.poulianas@titan.gr (N.P.); m.katsiotis@titanmaterials.com (M.S.K.)
* Correspondence: i.n.tsimpanogiannis@certh.gr

Abstract

One thermodynamic parameter that is crucial to heat transport within the fluidized bed inside the rotary kiln, during clinker production, is the specific heat capacity. The particular parameter is often considered constant in the open literature, while, in reality, it strongly depends on the fluidized bed's temperature and composition, considering that the temperature inside the kiln ranges from approx. 800 K up to 2000 K. For the current study, a mixing rule reported in the literature was applied in order to calculate the C_p of the fluidized bed, utilizing temperature and composition profiles available in the literature. An in-house code was developed for the comparison of the literature-reported C_ps and those resulting from the mixing rule. It was discovered that the C_p of the fluidized bed had a proportional increase with the increase in the temperature along the length of the kiln. The deviation between the two values (calculated and literature) is relatively small in some cases, whereas, in others, it is quite significant, ranging from 1.56% to 52.49%, thus making the adoption of the temperature-dependence of C_p necessary. Establishing a more accurate relation for the specific heat capacity leads to a better energy balance inside the kiln, which, along with other improvements, can lead to a decrease in the energy consumed and a significant reduction in greenhouse gas emissions.

Keywords: C_p calculation; cement rotary kiln; solid mixture; variable property; computational studies

Check for updates

Academic Editor: Sergei Manzhos

Received: 30 November 2025
Revised: 24 January 2026
Accepted: 29 January 2026
Published: 4 February 2026

Copyright: © 2026 by the authors. Licensee MDPI, Basel, Switzerland. This article is an open access article distributed under the terms and conditions of the Creative Commons Attribution (CC BY) license.

1. Introduction

The cement industry is one of the largest contributors to greenhouse gas emissions, while simultaneously being a very energy-intensive industry. Currently, the average energy consumption in more advanced rotary kilns (depending on the kiln type) is 3.5 GJ per ton clinker produced [1], a number that has improved due to the upgrades in kiln design and operational protocols that have been made over the years. In order to improve the kiln operation, it is important to study different parameters that can enhance energy efficiency and simultaneously preserve/enhance the quality of the final product.

Out of the total energy consumption in the cement industry, thermal energy accounts for approximately 80% of the primary energy consumption, with the electrical energy making up the remaining 20%. Depending on the type of the kiln (i.e., wet, dry, semi-dry), the above numbers can vary significantly [2] due to different percentages of moisture of the raw meal that needs to be evaporated. Typically, in the wet process kiln, the raw meal contains 36% moisture, while in the corresponding dry type, that percentage is only 0.5% [3]. In particular, the clinker production requires approximately 4 GJ per ton of clinker produced; however, depending on the kiln type, that amount can be reduced to 3.4 GJ/ton for the dry kiln, while it can increase up to 5.29 GJ/ton for the wet type [1]. For each ton of cement produced, an equivalent amount of gas emissions is released into the atmosphere [4]. In some countries with advanced plants for cement production, the energy consumption drops to 2.95 GJ/ton, whereas, on the other hand, the consumption can increase up to 5 GJ/ton if the cement plant is not well equipped [5–7]. In the US, the energy intensity of the cement industry improved from 4.45 GJ/ton in 1999 to 3.65 GJ/ton in 2009. Similar trends are followed by the data from the Cement Association of Canada, with the respective numbers being 3.91 GJ/ton in 2002 and 3.48 GJ/ton in 2010 [8–10]. In the work of Oda et al. [1], based on the type of the kiln and also on the existence of preheaters and pre-calciners, it was observed that the consumed thermal energy is proportional to the lower heating value. The highest consumption was found for the case of the wet-type kiln, while the lowest consumption belonged to the dry-type kiln coupled with 4 to 6 cyclone preheaters and a pre-calciner.

Figure 1 shows the time evolution of the thermal intensity of the clinker production in Europe and in the US, along with future projections based on indicators in the Reference Technology Scenario (RTS) and the roadmap vision (2DS). Similar information is also provided in Tables 1 and 2. It is evident that during recent years, a significant reduction has occurred, which is projected to be continued in the future as well.

The rotary kiln sector is considered to be the clinker production process's most polluting sector [2,3], as the emissions are carbon dioxide, nitrogen oxide, chlorofluorocarbons and methane (greenhouse effect gases) [4,5]. A well-designed rotary kiln is essential as it can reduce emissions and improve energy efficiency while preserving the final product quality. The rotary kiln under investigation in the current study is of the dry type, so its energy consumption is already lower than that of the corresponding wet-type kiln. Nevertheless, kiln parameters, along with those in the energy balance equation, must be optimized in order to reduce greenhouse-gas emissions and energy consumption. The fluidized bed's specific heat capacity, C_p, is a parameter that can have a significant effect on the total energy consumption in the rotary kiln. Also, another factor that can be improved is the rotational speed of the kiln, as previous studies have shown that it can increase the convection heat transfer coefficient [6–8].

Table 1. Energy consumption in different cement kilns in chronological order.

Year	Source	Country	Energy Per Type of Process [GJ/ton Clinker]	
			Wet	Dry
1994	[9]	U.S.	366 PJ total	-
2002	[10–12]	Global	5.3–7.1	3.06
2006	[13]	Global	6.38	3.55
2006	[13,14]	Global	-	3.42
2007	[5]	U.S.	6.5	5.3
2011, 2017	[15,16]	Asia	5.68–6.28	4.6
2014	[17]	Global	-	3.5
2020	[3]	Iran	-	3.4
2022	[18]	Global	5.29	3.4

Table 2. Specific thermal energy by technology [19] (European Commission). n.a.: not available.

Technology	Specific Thermal Energy Demand	
	[MJ/ton Clinker]	Weighted Average [MJ/ton Clinker]
Dry kiln with preheater and pre-calciner	3000 < 4000	3515
Dry kiln with preheater without pre-calciner	3100 to 4200	3700
Semi-wet/semi-dry process	3300 to 5400	3918
Dry kiln without preheater (long dry kiln)	Up to 5000	3570
Wet process	5000 to 6400	5512
Shaft kilns	3100 to 6500 and higher	n.a.

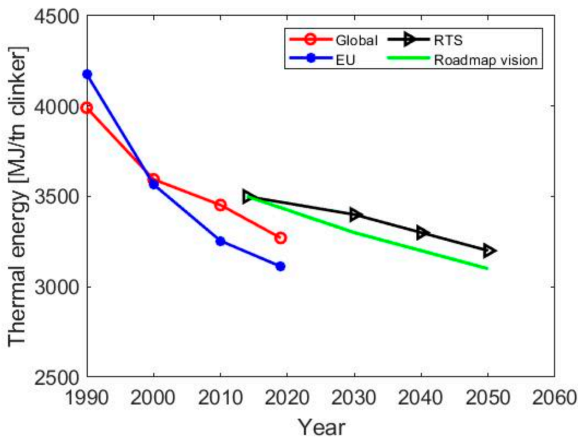

Figure 1. Clinker thermal energy intensity in EU27 and at global level (MJ/ton clinker) [19] along with key indicators in the RTS (Reference Technology Scenario) and the roadmap vision (2DS).

During the current study, it was observed that a common assumption encountered in most published studies considering the modeling of rotary cement kilns was that the specific heat capacity of the fluidized bed was kept constant throughout the process. The particular assumption was ubiquitous, even though the temperatures inside the rotary kiln can range from approximately 800 K in the kiln inlet to almost 2000 K near the burner. Besides the chemical reactions and their corresponding kinetic parameters, the process is also affected by additional factors such as the heat transfer between all the phases (i.e., fluidized bed, gas, and solid kiln), the wall of the kiln, and the technical features of the kiln itself. While testing different case scenarios from the literature, via "in-house" codes, in order to find the optimal parameters, it was identified that the use of variable values of C_p has an impact on the concentration profiles of the components as a function of the kiln length. Additional research was conducted on this matter, as most of the literature sources suggested the use of a constant value for the bed heat capacity, thus ignoring the variability of C_p.

Therefore, the main objective/motivation of the current study is to examine the validity of the assumption of using constant values for C_p along the rotary kiln (i.e., independent of the temperature profile). To this purpose, the literature-reported temperature and compositional profiles along the length of the rotary kiln are utilized and are coupled with a mixing rule for C_p. Calculations (accounting for temperature and compositional variations along the kiln length) are performed in order to quantify the difference between variable and constant C_ps, and significant deviations are identified.

2. Methodology

The raw material in the kiln inlet consists of a mixture of clay and finely ground limestone that is processed inside the kiln to produce clinker. The main compounds of clinker minerals are the dicalcium silicate [$2CaO{\cdot}SiO_2$ (Belite): denoted as C_2S], tricalcium silicate [$3CaO{\cdot}SiO_2$ (Alite): denoted as C_3S], tricalcium aluminate [$3CaO{\cdot}Al_2O_3$ (Aluminate): denoted as C_3A], and tetracalicium aluminoferrite [$4CaO{\cdot}Al_2O_3{\cdot}Fe_2O_3$ (Ferrite): denoted as C_4AF], which are also the main products of the reactions taking place in the rotary kiln [20,21]. High temperatures are necessary for the initiation of those reactions. Certain assumptions are often made for problem simplification. Typical assumptions reported in the literature are summarized below:

- The system is assumed to be in a steady state with constant flow [22].
- The model is considered one-dimensional (1D).
- The fluidized bed height remains constant along the entire length of the kiln [23].
- The fluidized bed is assumed to move transversely within the cement rotary kiln, allowing it to be treated as a plug flow reactor (PFR) [23,24].
- The decomposition of calcium carbonate is assumed to take place primarily in the pre-calciner, so the CO_2 source term of the energy equation can be ignored for the case of the rotary kiln.
- The chemical reactions are restricted to five main ones (shown in Table 3) with corresponding kinetics [25–28] whose reaction rate is determined by an Arrhenius-type law with fixed values in the enthalpies of the reactions, the latent heat of the solid, activation energies and pre-exponential factors remain constant.
- The rotary kiln is a dry-type kiln; therefore, heat transfer from H_2O release due to low moisture content in the raw material is ignored [29,30].
- The emission factors are assumed to remain constant over the entire length of the rotary kiln for the gas phase, the fluidized bed and the inner wall.

A schematic of the cross-sectional area of the rotary kiln is shown in Figure 2.

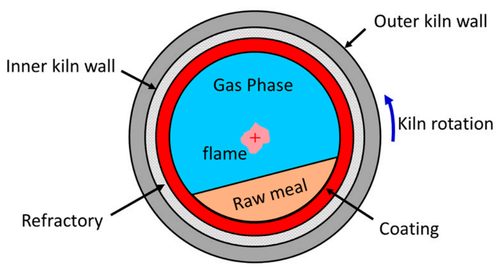

Figure 2. Cross-sectional area of the rotary cement kiln.

In the current study, the reactions occurring in the fluidized bed were limited to 5 main reactions with their respective temperature range indicated in Table 3. In order to calculate the C_p of the fluidized bed, it is necessary (i) to find an expression that describes the dependence of C_p on temperature for each one of the nine primary chemical components that participate in the chemical reactions shown in Table 3, (ii) to obtain an expression (i.e., mixing rule) for the composite fluidized bed, and (iii) to take into account the concentration changes in each component along the kiln length.

Table 3. Main reactions of clinkerization inside the rotary kiln [31].

	Reactions	Temperature Range [K]
1	$CaCO_3 \rightarrow CaO + CO_2$	823–1233
2	$2CaO + SiO_2 \rightarrow C_2S$	873–1573
3	$C_2S + CaO \rightarrow C_3S$	1473–1553
4	$3CaO + Al_2O_3 \rightarrow C_3A$	1453–1553
5	$4CaO + Al_2O_3 + Fe_2O_3 \rightarrow C_4AF$	1453–1553
6	$Clinker_{(sol)} \rightarrow Clinker_{(liq)}$	>1553

Based on the chemical reactions scheme, shown in Table 3, there are nine solid components that participate as either reactants or products, given here for practical reasons, as two distinct groups:

- Group A: $CaCO_3$, CaO, SiO_2, Al_2O_3, and Fe_2O_3.
- Group B: C_2S, C_3S, C_3A, and C_4AF.

In the following sections, the equations that have been used in the current study for the calculation of C_p are provided.

2.1. Calculations of C_p for Components of Group A

For all the components belonging to Group A, the component-specific equations of C_p as a function of temperature were obtained from Perry's Handbook [32]. Namely:

- $CaCO_3$

$$C_p = 19.68 + 0.01189T - \frac{307,600}{T^2} \quad 273\text{ K} < T < 1033\text{ K} \tag{1}$$

- CaO

$$C_p = 10 + 0.00484T - \frac{108,000}{T^2} \quad 273\text{ K} < T < 1173\text{ K} \tag{2}$$

- SiO_2

$$\begin{array}{lll} C_p = 10.87 + 0.008712T - \frac{241,200}{T^2} & 273\text{ K} < T < 848\text{ K} & \text{c, quartz a} \\ C_p = 10.95 + 0.00550T & 848\text{ K} < T < 1873\text{ K} & \text{c, quartz } \beta \end{array} \tag{3}$$

- Al_2O_3

$$C_p = 22.08 + 0.008971T - \frac{522,500}{T^2} \quad 273\text{ K} < T < 1973\text{ K} \tag{4}$$

- Fe_2O_3

$$C_p = 24.72 + 0.01604T - \frac{423,400}{T^2} \quad 273\text{ K} < T < 1097\text{ K} \tag{5}$$

Also, similar equations for the cases of CaO, Al_2O_3, and SiO_2 (i.e., components belonging to Group A) were obtained from Haas Jr et al. [33].

- CaO

$$C_p = \frac{-2.55577\times10^5}{T^2} - \frac{4.31990\times10^2}{T^{0.5}} + 71.6851 - 2\times3.08248\times10^{-3}T + 2.23862\times10^{-6}T^2 \quad 273\text{ K} < T < 1800\text{ K} \tag{6}$$

- Al_2O_3

$$C_p = \frac{-2.46518\times10^3}{T^{0.5}} + 2.33004\times10^2 - 2\times1.95913\times10^{-2}T + 9.44410\times10^{-6}\,T^2 \quad 273\text{ K} < T < 1800\text{ K} \tag{7}$$

- SiO_2, quartz a

$$C_p = \frac{-7.77338\times10^2}{T^2} + 83.2101 + 2\times1.09962\times10^{-2}T \qquad 273\text{ K} < T < 844\text{ K} \tag{8}$$

- SiO_2, quartz β

$$C_p = 58.9107 + 2\times5.0208\times10^{-3}T \qquad 844\text{ K} < T < 1800\text{K} \tag{9}$$

The behavior of Equations (1)–(6) is demonstrated as a function of temperature using the equations from Perry's handbook in the figures below. In particular, Figure 3a shows C_p within the temperature range where the equations are applicable, while Figure 3b shows C_p at temperature conditions that are extrapolated to those that the rotary cement kiln operates. Similarly, Figure 4a,b show the same results utilizing the equations from Haas Jr. et al. [33].

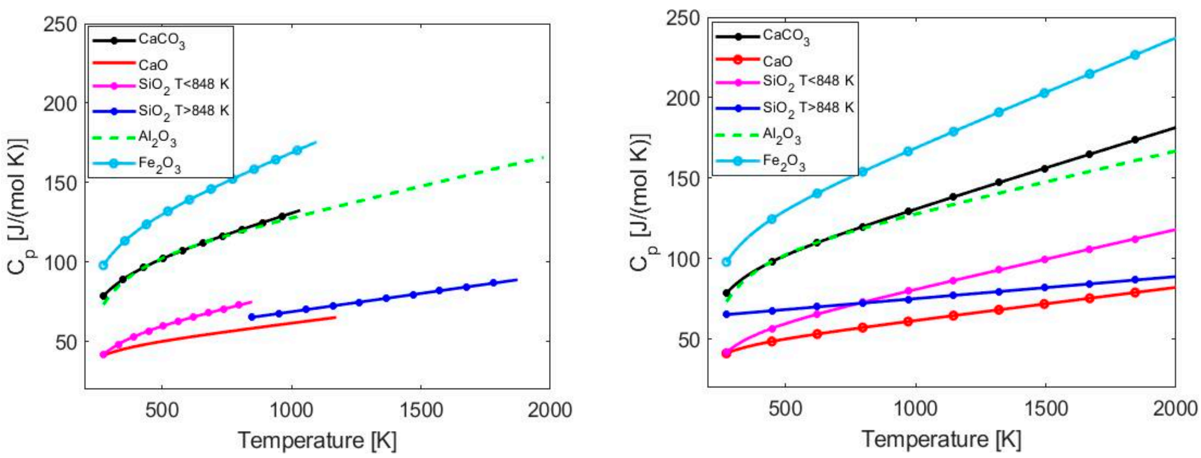

(a) (b)

Figure 3. Calculated C_p values as a function of temperature using the equations from Perry's handbook [32]. C_p within the temperature range where the equations are applicable (**a**) and C_p at extrapolated temperature conditions (**b**).

Although the temperature range of applicability of the equations provided by Haas Jr. et al. [33] was closer to the kiln operating conditions, the calculations in the current study were performed using the equations from Perry's handbook, as the missing information for the nine components was less (i.e., for self-consistency reasons). In particular, Perry's handbook provided information for all components (5/5) of Group A, while Haas Jr. et al. provided information for only 3 out of 5 components (3/5) of Group A. Neither option provided information for components of Group B.

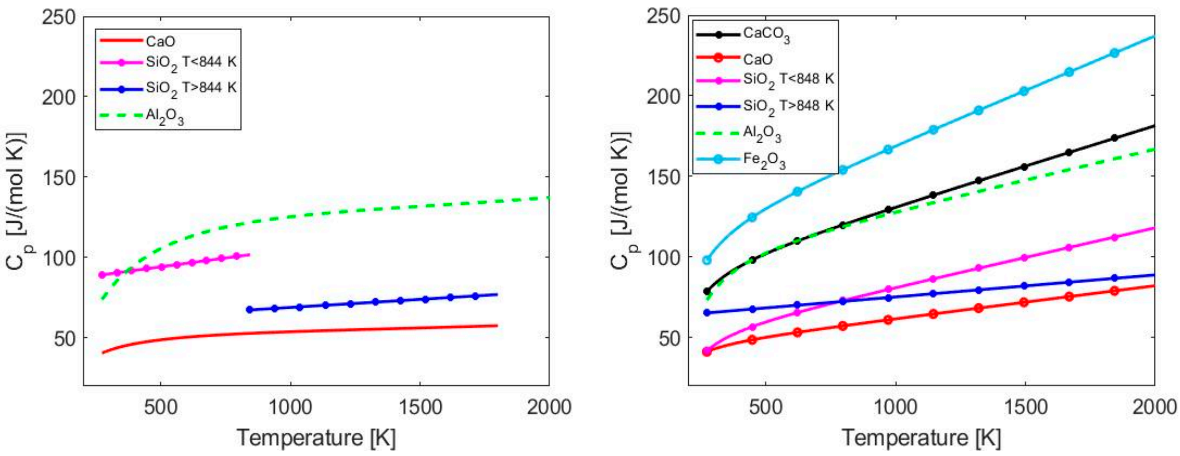

(**a**) (**b**)

Figure 4. Calculated C_p values using equations from Haas Jr. et al. [33]. C_p within the temperature range of equation development (**a**), and C_p at extrapolated temperature conditions (**b**).

2.2. Calculations of C_p for Components of Group B

On the other hand, for the case of C_2S, C_3S, C_3A and C_4AF (i.e., Group B components), there is no data (either experimental or computational) available for the temperature dependence of C_p. Members of Group B are intermediate chemical components, appearing at locations along the rotary kiln, which are hard to isolate and sample, and thus really challenging to measure experimentally their corresponding C_p's. Instead, Mai et al. [34] provided information for the specific heat under constant volume (C_v) within the temperature range of 0 up to 800 K. The specific heat capacity under constant volume was calculated by Mai et al. [34] via the Density Functional Theory (DFT) method [35], which is a computational quantum mechanical modeling technique.

In order to proceed, we recall from Thermodynamics that the relation between C_p and C_v is given by

$$C_p - C_v = \frac{T\alpha^2}{\rho\beta} \tag{10}$$

where ρ is the density of the mixture calculated with atomistic simulations, α is the thermal expansion coefficient, and β is the compressibility of the bulk modulus. Those coefficients are given, respectively, from the relations below [36]:

$$\alpha = \frac{1}{V}\left(\frac{\partial V}{\partial T}\right)_P \tag{11}$$

$$\beta = \frac{1}{V}\left(\frac{\partial V}{\partial P}\right)_T \tag{12}$$

For ideal gases, the relation between C_p and C_v is given as $C_p - C_v = R$ but, when it comes to solids or liquids, the value of $C_p - C_v$ is so small that it can be considered negligible for most cases [36], as solids are considered incompressible, while liquids have limited compressibility. Therefore, for the aforementioned components, it is assumed, in the current study, that the C_v value is equal to the C_p value.

Next, the specific heat capacity under constant volume (C_v), reported by Mai et al., for the products of the chemical reactions, is plotted in Figure 5 as a function of temperature. Furthermore, the calculated values are fitted (in the temperature range 200–800 K) using Equation (14), and the resulting curves are shown in Figure 6. Each curve fitting is described by the following equation:

$$y = a_1 \ln(x) + a_0 \tag{13}$$

where the calculated parameters a_0, a_1 are shown in Table 4, along with the coefficient of determination R^2, which indicates the goodness of the fit.

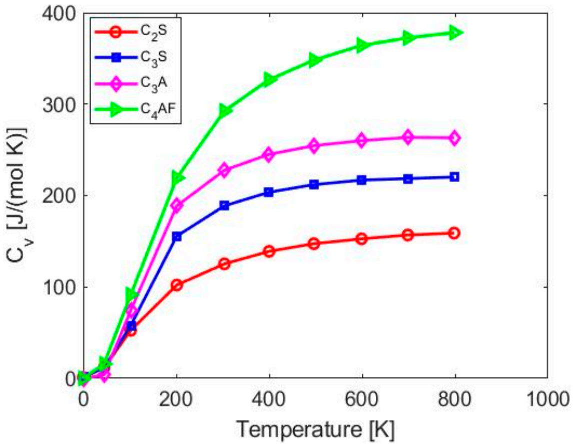

Figure 5. Specific heat capacity at constant volume, C_v, for C_2S, C_3S, C_3A, and C_4AF as a function of temperature, obtained from the literature [34]. Solid lines connecting the data points are guides to the eye only.

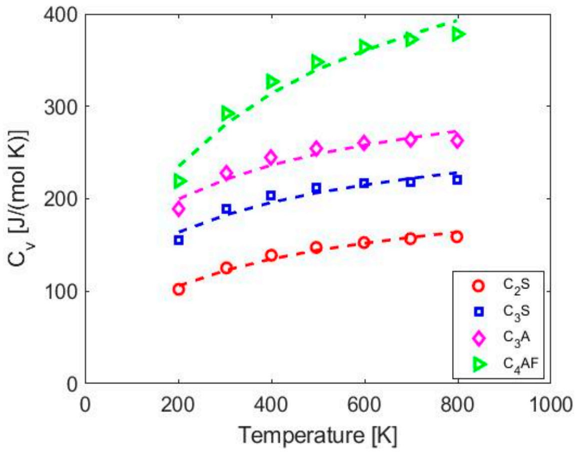

Figure 6. Symbols denote data from the literature for specific heat capacity at constant volume (obtained from [34]), while dashed lines of the same color denote the fitted curves (this work).

Table 4. Constants of the curve equations.

Components	a_1	a_0	R^2
C_2S	41.774	−115.4	0.9642
C_3S	46.334	−81.538	0.9108
C_3A	52.824	−80.033	0.9125
C_4AF	113.6	−366.6	0.9546

In Figure 5, below, it can be observed that the C_v of the four components belonging to Group B remain relatively constant at temperatures higher than approx. 400 K. Therefore, for engineering-type calculations, it can be assumed that for such temperatures, the C_v value of each component of Group B remains constant.

In conclusion, for the aforementioned four components of Group B, it is assumed, in the current study, that the C_v value is equal to the C_p value and remains constant for temperatures above 800 K, following the asymptotic value corresponding to this temperature. This assumption is critical because inside the rotary cement kiln, the temperature ranges between approx. 800 and 2000 K [37].

2.3. Calculations of C_p for the Mixed Fluidized Bed

Considering that energy and volume are extensive thermodynamic quantities, in a mixture, they can be expressed as a sum of the individual quantities. So, the specific heat capacity at constant pressure can be written as a linear combination of the individual phases [38]. Combining the heat capacities of pure components from both the equations and the diagrams with the compositions of the components along the kiln that were taken from the literature, it becomes possible to calculate the needed parameter.

The mixing rule for the calculation is based on the work of Abdolhosseini Qomi et al. [38], given as follows:

$$C_{p,mix} = (1-n)\sum_{i=1}^{m} \Phi_{Ri} C_{p,Ri} + n\sum_{i=1}^{m} \Phi_{Pi} C_{p,Pi} \quad (14)$$

where m is the number of reactive agents, and n is the reaction degree. Φ_{Ri}, and Φ_{Pi} represent the mass fractions of the reactants (denoted with subscript Ri) and the products (denoted with subscript Pi), respectively, and C_{pi} are the heat capacities of the pure components. Applying all the known information (the heat capacities of pure components and the concentrations along the kiln) in Equation (14), the C_p of the solid mixture can be calculated. Given that there are five reactions in the system rather than just one, the rotary kiln can be divided into small, nearly equal sections where the temperature is kept constant, and the compositions are either reactants of the subsequent step or products of the previous step, simplifying the reaction degree to either 1 or 0 in each instance. Shown in Figure 7 is a schematic of the discretization along the length of the rotary kiln.

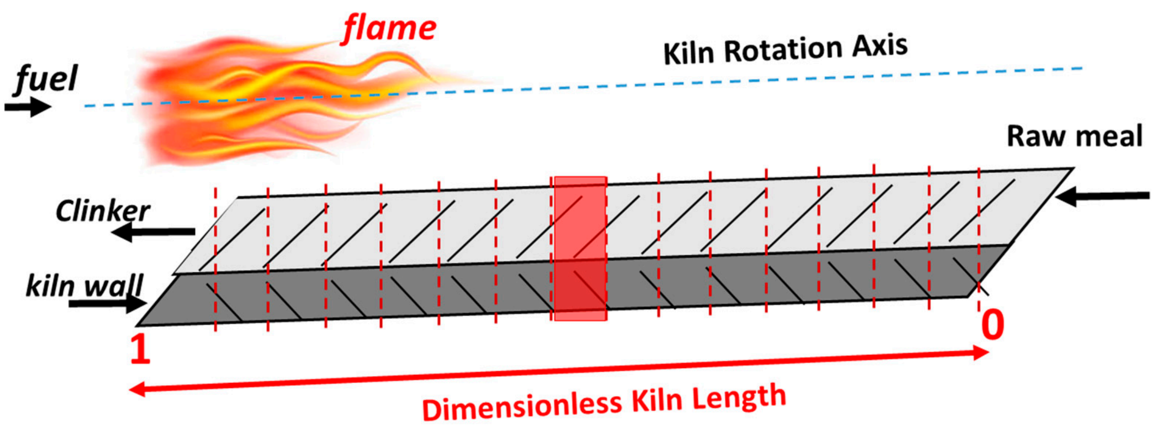

Figure 7. Schematic of the discretization along the length of the rotary kiln.

3. Results and Discussion

Table 5 shows a list of computational studies (in chronological order) reporting temperature and compositional profiles along the rotary kiln length.

For all calculations performed in the current study, in-house codes have been utilized, and the obtained results are shown in the following figures. At first, calculations were performed using the units of the mixing rule equation (i.e., [J/(mol K)]); however, in order to be consistent with the literature values for C_p, the units were subsequently converted to [J/(kg K)].

Table 5. Literature sources in chronological order reporting temperature and compositional profiles. The last column indicates the particular chemical species for which the compositional profile was not reported in the original studies. [-] indicates that the compositional profiles for all nine components are reported in the original studies.

Authors	Year	Ref. Source	Missing Component
Spang et al.	1972	[39]	Al_2O_3; Fe_2O_3
Mastorakos et al.	1999	[37]	[-]
Mujumdar et al.	2006	[22]	SiO_2; Al_2O_3; Fe_2O_3
Mujumdar et al.	2006	[23]	SiO_2; Al_2O_3; Fe_2O_3
Darabi et al.	2007	[24]	SiO_2; Al_2O_3; Fe_2O_3
Csernyei et al.	2016	[31]	SiO_2; Al_2O_3; Fe_2O_3
Colina-Morles et al.	2016	[25]	Fe_2O_3
Gonzales et al.	2016	[26]	[-]
Abdelwahab et al.	2017	[27]	[-]
Pieper et al.	2020	[28]	SiO_2; Al_2O_3; Fe_2O_3
Mungyeko Bisulandu and Marias	2021	[21]	[-]

Figure 8 shows the parameters of interest to the current study plotted in four subfigures, resulting from the calculations based on the work of Mastorakos et al. [37]. In particular, Figure 8a shows the reported solid bed temperature profile along the dimensionless kiln length, while Figure 8b shows the corresponding solid bed composition, expressed as mass fractions, along the dimensionless kiln length. Figure 8c shows the current calculated C_p of the solid mixture of the kiln bed in units of [J/(mol K)]. The calculated C_p values are plotted along the dimensionless kiln length, taking into account the temperature profile as well. Finally, Figure 8d demonstrates the comparison of the current calculated (denoted with red circles) C_p (converted in units of [J/(kg K)]) and the values used by Mastorakos et al. [37]. Figure 8d also indicates, for a limited number of characteristic locations along the rotary kiln length, the % *dev.* between the calculated C_p^{curent} in the current study and the $C_p^{lit.}$ value reported by the authors in their original publication. % *dev.* is defined as follows: $\%\,dev. = 100 \times \left(\frac{C_p^{curent} - C_p^{lit.}}{C_p^{curent}}\right)$. Therefore, negative values for the % *dev.* indicate an under prediction of the current study, while positive values indicate an over prediction.

Figures 9–11 show the corresponding results for the cases of the studies of González et al. [26] (Figure 9), Abdelwahab et al. [27] (Figure 10), and Mungyeko Bisulandu and Marias [21] (Figure 11). Results are presented only for these particular four cases among all cases included in Table 5. The four cases report info for the compositional evolution along the kiln for all nine components that are involved in the process.

An interesting observation from the current analysis is that every source in the open literature provides different composition and temperature profiles, and also different sets of operational rotary kiln parameters. Furthermore, as Table 6 indicates, there is a wide range of C_p values that have been used in the open literature. On the other hand, in the current study, for each system, there is a proportional increase in C_p with increasing temperature compared to the literature values, which remain constant throughout the process. The particular observations indicate that there is a need for the systematic analysis of the effect of errors on the overall energy balance of the rotary kiln and the resulting temperature and compositional profiles. However, since no systematic error analysis is provided in the earlier studies, such an effort is far beyond the scope of the current study and is left for the future.

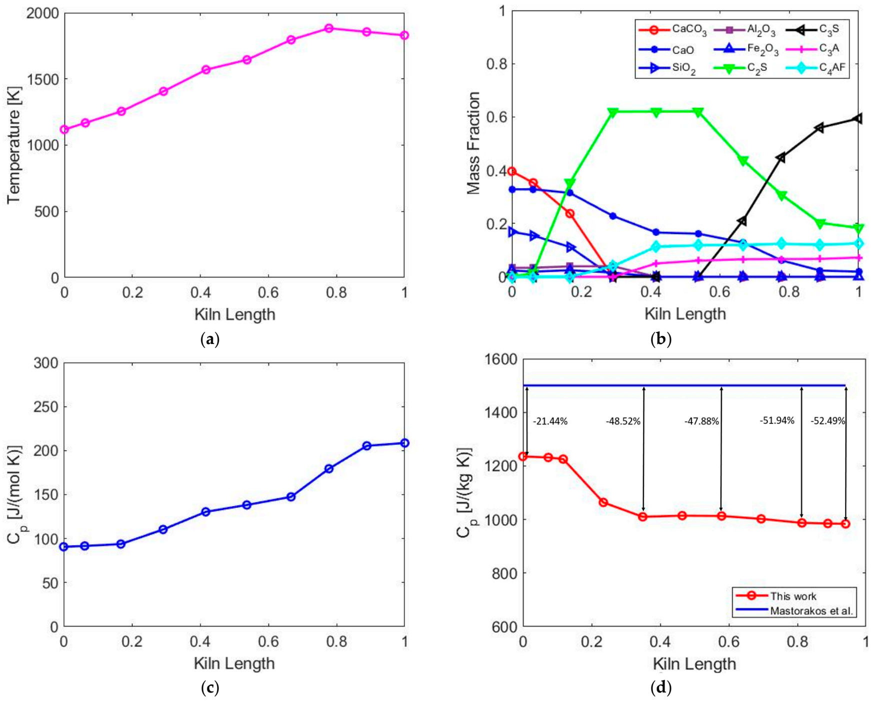

Figure 8. Different parameters plotted as a function of the dimensionless rotary kiln length. Literature data (Mastorakos et al., [37]) for: (**a**) solid bed temperature, and (**b**) solid bed composition expressed as mass fraction. (**c**) Calculated C_p of the solid mixture of the kiln bed in [J/(mol K)]. (**d**) Comparison of the calculated (denoted with red circles) C_p (in [J/(kg K)]) and the value used by Mastorakos et al. [37] (denoted with the solid blue line). Solid lines connecting the symbols are guides to the eye only.

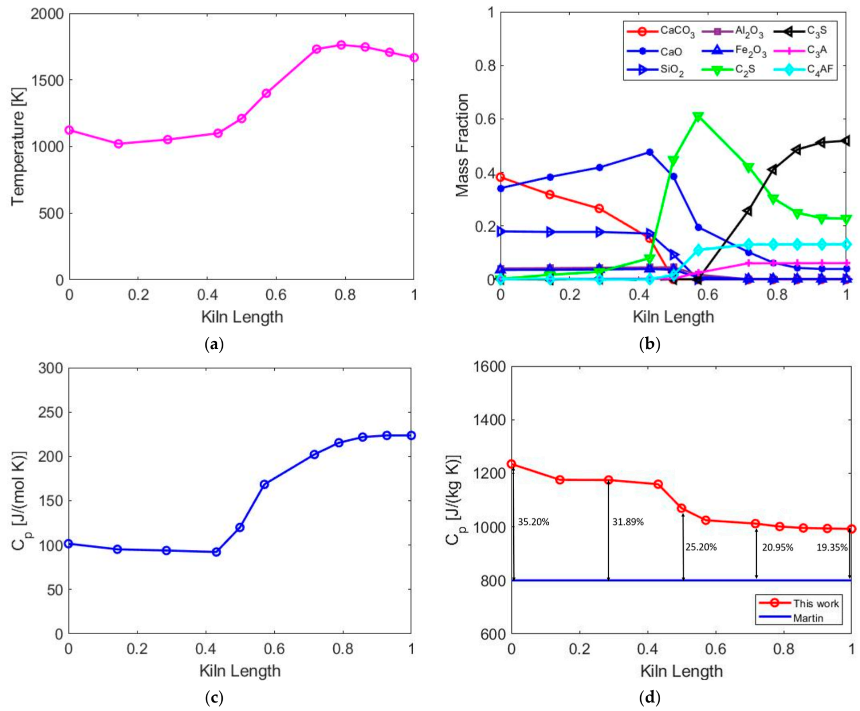

Figure 9. Different parameters plotted as a function of the dimensionless rotary kiln length. Data from the literature (González et al., [26]) for: (**a**) solid bed temperature, and (**b**) solid bed composition expressed as mass fraction. (**c**) Calculated C_p of the solid mixture of the kiln bed in [J/(mol K)]. (**d**) Comparison of the calculated (denoted with red circles) C_p (in [J/(kg K)]) and the value used by González et al. (Martin, [9], denoted with the solid blue line). Solid lines connecting the symbols are guides to the eye only.

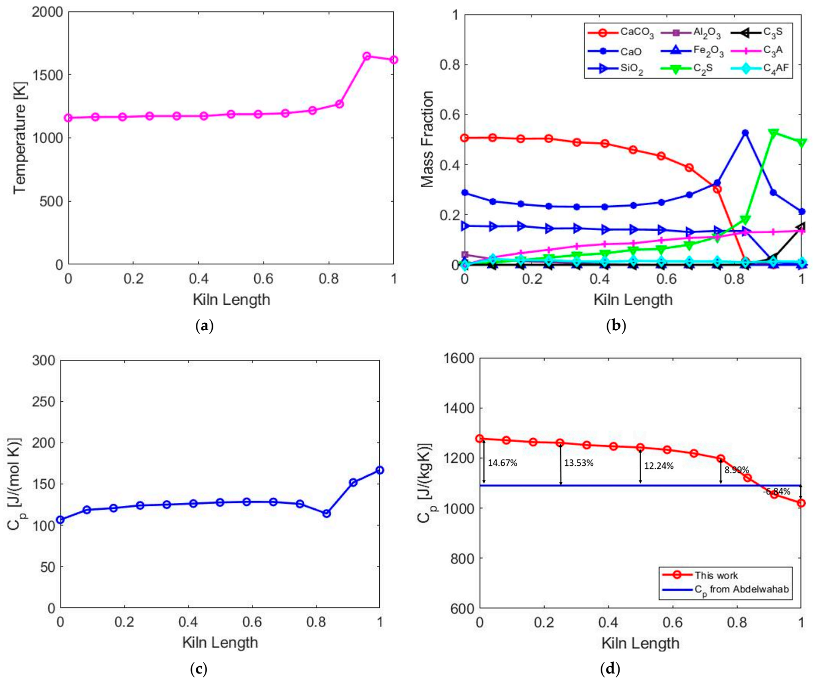

Figure 10. Different parameters plotted as a function of the dimensionless rotary kiln length. Data from the literature (Abdelwahab et al., [27]) for: (**a**) solid bed temperature, and (**b**) solid bed composition expressed as mass fraction. (**c**) Calculated C_p of the solid mixture of the kiln bed in [J/(mol K)]. (**d**) Comparison of the calculated (denoted with red circles) C_p (in [J/(kg K)]) and the value used by Abdelwahab et al. [27] (denoted with the solid blue line). Solid lines connecting the symbols are guides to the eye only.

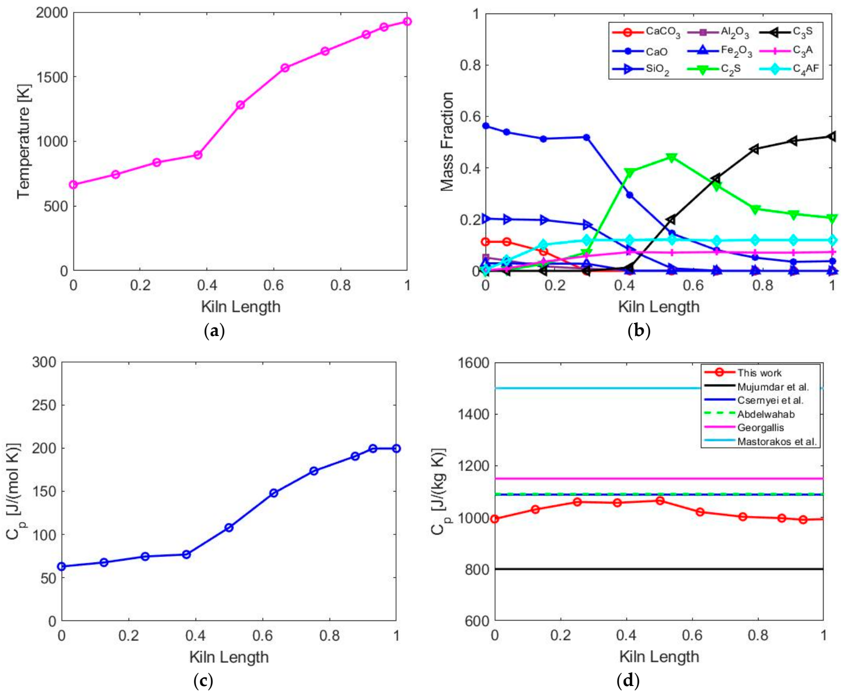

Figure 11. Different parameters plotted as a function of the dimensionless rotary kiln length. Data from the literature (Mungyeko Bisulandu and Marias, [21]) for: (**a**) solid bed temperature, and (**b**) solid bed composition expressed as mass fraction. (**c**) Calculated C_p of the solid mixture of the kiln bed in [J/(mol K)]. (**d**) Comparison of the calculated (denoted with red circles) C_p (in [J/(kg K)]) and various constant values from the literature (Cserney et al. [31]; Mastorakos et al. [37]; Mujumdar et al. [22]; Abdelwahab et al. [27]; Georgalis [30]). Solid lines connecting the symbols are guides to the eye only.

Table 6. Literature-reported values for C_p.

Literature Source	C_p [J/(kg K)]
Pieper et al. [28]	Polynomial for SiO_2
Mastorakos et al. [37]	1500
Mungyeko Bisulandu and Marias [21]	-
Colina-Morles et al. [25]	C_p solids relation [$C_s = 1000 \times (0.88 + 0.000293\ T_s)$]
Mujumdar et al. [22]	800
Csernyei et al. [31]	1088 (from Darabi [24])
Darabi [24]	1088
Gonzales et al. [26]	800 (from Mujumdar et al. [22])
Abdelwahab et al. [27]	1090
Georgallis [30]	1150

From Figures 8–11, we observe that the variable C_p values calculated in the current study range between 1000 and 1300 [J/(kg K)]. Depending on the constant value for C_p used in the original studies, we estimated that the % *dev.* can range between 21 and 53% (underestimation) for the case of Mastorakos et al., 19–35% (overestimation) for the case of González et al., and 7% (underestimation) up to 15% (overestimation) for the case of Abdelwahab et al. It should be pointed out that for the case of Mungyeko Bisulandu and Marias (e.g., see Figure 11d), the C_p value used was not reported in that study. Therefore, in Figure 11d, the constant C_p values from various literature sources (i.e., five cases) are also indicated with the constant horizontal lines. As a result, the % *dev.* between the calculated C_p^{curent} values of the current study and the $C_p^{lit.}$ value can be calculated for all five cases. Such results are shown in Figure 12.

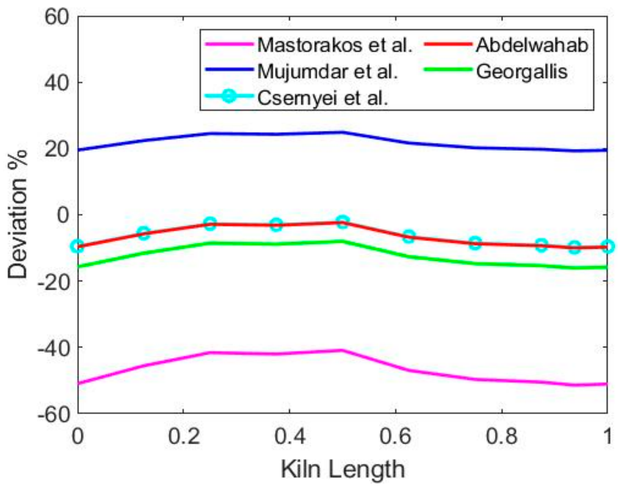

Figure 12. Analysis of the simulation results of Mungyeko Bisulandu and Marias [21]. % dev. between the calculated C_p^{curent} values of the current study and the constant $C_p^{lit.}$ value from various sources (Cserneyi et al. [31]; Mastorakos et al. [37]; Mujumdar et al. [22]; Abdelwahab et al. [27]; Georgallis [30]).

4. Conclusions and Future Outlook

Energy consumption differs depending on the type of kiln, as a wet process kiln requires more thermal and electrical energy due to the higher amount of moisture in the raw meal in comparison with a dry process [8]. From the calculations reported in the current study, it can be concluded that the heat capacity of the fluidized bed varies along the kiln length as a result of changes in composition and temperature. The calculated values fluctuate within a range, as the extracted information for the reported concentration profiles exhibits inconsistencies, and several parameter values used were not fully aligned. Since there is a strong dependence on the temperature and the composition for the calculated C_p, according to the applied mixing rule, it is concluded that during the simulations, the value of C_p should not be considered constant along the kiln length. Instead, using a position-dependent (corresponding to different temperatures along the rotary kiln) C_p is recommended. Incorporating a more realistic value of C_p along the kiln influences the system behavior and, in particular, the composition profiles of clinker along the process. Establishing a more accurate description of the specific heat capacity improves the energy balance inside the kiln and, along with other enhancements, can lead to a decrease in the energy consumed and to a further reduction in greenhouse gases. Thus, for more reliable predictions of the compositions and the temperature inside a rotary kiln, a variable C_p should be used. Another observation is that, in all examined cases, there is a proportional increase in the values of C_p with the increase in temperature, in contrast to constant literature values. Finally, yet importantly, although the deviation between the literature and the calculated values is relatively small, in some instances it becomes quite significant, fluctuating from 1.56% up to 52.49%, clearly demonstrating the dependence on temperature.

Author Contributions: Conceptualization, E.K. and I.N.T.; methodology, E.K. and I.N.T.; software, E.K., M.M., A.K. and T.K.; validation, E.K., M.M., A.K., T.K., A.T. and I.N.T.; formal analysis, E.K., M.M., A.T., V.K.M. and I.N.T.; investigation, E.K., E.G., M.M., A.K. and T.K.; resources, E.K., E.G., M.M., T.D., G.S., A.K., T.K., A.T., V.S., N.P., M.S.K., A.A. and I.N.T.; data curation, E.K.; writing—original draft preparation, E.K. and I.N.T.; writing—review and editing, E.G., M.M., T.D., G.S., A.K., T.K., A.T., V.K.M., V.S., N.P., M.S.K. and A.A.; visualization, E.K., M.M., T.D., A.K. and T.K.; supervision, A.T., V.K.M., A.A. and I.N.T.; project administration, A.T., V.K.M., M.S.K. and A.A.; funding acquisition, G.S., A.T., V.K.M., M.S.K. and I.N.T. All authors have read and agreed to the published version of the manuscript.

Funding: This research was funded by the project “DigiKiln” (project code: KMP6-0079905) under the framework of the Action “Investment Plans of Innovation” of the Operational Program “Central Macedonia 2014–2020”, which is co-funded by the European Regional Development Fund (ERDF) of the European Union and Greece.

Institutional Review Board Statement: Not applicable.

Informed Consent Statement: Not applicable.

Data Availability Statement: Dataset available on request from the authors.

Conflicts of Interest: Authors V. Michalis, V. Stroungaris, N. Poulianas, and M. Katsiotis were employed by the cement company TITAN Cement S.A. The remaining authors declare that the research was conducted in the absence of any commercial or financial relationships that could be construed as potential conflicts of interest.

Abbreviations

The following abbreviations are used in this manuscript:

C_2S	dicalcium silicate: $2CaO{\cdot}SiO_2$ (Belite)
C_3S	tricalcium silicate: $3CaO{\cdot}SiO_2$ (Alite)
C_3A	tricalcium aluminate: $3CaO{\cdot}Al_2O_3$ (Aluminate)
C_4AF	tetracalicium aluminoferrite: $4CaO{\cdot}Al_2O_3{\cdot}Fe_2O_3$ (Ferrite)
DFT	Density Functional Theory
MC	Monte Carlo
MD	Molecular dynamics
PFR	Plug flow reactor

References

1. Oda, J.; Akimoto, K.; Tomoda, T.; Nagashima, M.; Wada, K.; Sano, F. International comparisons of energy efficiency in power, steel, and cement industries. *Energy Policy* **2012**, *44*, 118–129. [CrossRef]
2. Atmaca, A.; Yumrutaş, R. Analysis of the parameters affecting energy consumption of a rotary kiln in cement industry. *Appl. Therm. Eng.* **2014**, *66*, 435–444. [CrossRef]
3. Mujumdar, K.S.; Ganesh, K.V.; Kulkarni, S.B.; Ranade, V.V. Rotary Cement Kiln Simulator (RoCKS): Integrated modeling of pre-heater, calciner, kiln and clinker cooler. *Chem. Eng. Sci.* **2007**, *62*, 2590–2607. [CrossRef]
4. Mokrzycki, E.; Uliasz-Bocheńczyk, A.; Sarna, M. Use of alternative fuels in the Polish cement industry. *Appl. Energy* **2003**, *74*, 101–111. [CrossRef]
5. Van Oss, H.G. Reducing cement's CO_2 footprint. *Priv. Sect. Dev.* **2011**, *10*, 12–15. Available online: https://www.proparco.fr/en/article/reducing-cements-co2-footprint (accessed on 20 December 2023).
6. Bohan, R.P. Heat transfer in rotary kilns: A retrospect. In *Proceedings of the 2016 IEEE-IAS/PCA Cement Industry Technical Conference, Dallas, TX, USA, 13–20 May 2016*; IEEE: New York, NY, USA, 2016; pp. 1–6. [CrossRef]
7. Sadighi, S.; Shirvani, M.; Ahmad, A. Rotary cement kiln coating estimator: Integrated modelling of kiln with shell temperature measurement. *Can. J. Chem. Eng.* **2011**, *89*, 116–125. [CrossRef]
8. Tscheng, S.H.; Watkinson, A.P. Convective heat transfer in a rotary kiln. *Can. J. Chem. Eng.* **1979**, *57*, 433–443. [CrossRef]
9. Martin, N.; Worrell, E.; Price, L. *Energy Efficiency and Carbon Dioxide Emissions Reduction Opportunities in the U.S. Cement Industry*; Lawrence Berkeley National Laboratory: Berkeley, CA, USA, 1999.
10. WBCSD. *Toward a Sustainable Cement Industry*; Climate Change; WBCSD: Geneva, Switzerland, 2002.
11. Taylor, M.; Tam, C.; Gielen, D. Energy Efficiency and CO_2 Emissions from the Global Cement Industry. In Proceedings of the IEA-WBCSD Workshop, Paris, France, 4–5 September 2006.
12. Ishak, S.A.; Hashim, H. Low carbon measures for cement plant—A review. *J. Clean. Prod.* **2015**, *103*, 260–274. [CrossRef]
13. Benhelal, E.; Zahedi, G.; Shamsaei, E.; Bahadori, A. Global strategies and potentials to curb CO_2 emissions in cement industry. *J. Clean. Prod.* **2013**, *51*, 142–161. [CrossRef]
14. Mirzakhani, M.A.; Tahouni, N.; Panjeshahi, M.H. Energy benchmarking of cement industry, based on Process Integration concepts. *Energy* **2017**, *130*, 382–391. [CrossRef]
15. International Finance Corporation. *Improving Thermal and Electric Energy Efficiency at Cement Plants*; World Bank: Washington, DC, USA, 2017. [CrossRef]
16. Madlool, N.A.; Saidur, R.; Hossain, M.S.; Rahim, N.A. A critical review on energy use and savings in the cement industries. *Renew. Sustain. Energy Rev.* **2011**, *15*, 2042–2060. [CrossRef]
17. IEA. *Technology Roadmap—Low-Carbon Transition in the Cement Industry*; IEA: Paris, France, 2018. Available online: https://www.iea.org/reports/technology-roadmap-low-carbon-transition-in-the-cement-industry (accessed on 20 December 2023).
18. Sahoo, N.; Kumar, A.; Samsher. Review on energy conservation and emission reduction approaches for cement industry. *Environ. Dev.* **2022**, *44*, 100767. [CrossRef]
19. Marmier, A. *Decarbonisation Options for the Cement Industry*; Publications Office: Luxembourg, 2023. Available online: https://publications.jrc.ec.europa.eu/repository/handle/JRC131246 (accessed on 20 December 2023).
20. Mungyeko Bisulandu, B.-J.R.; Pongo, P.C. Les énergies renouvelables face à l'épuisement des énergies fossiles: Utilisation et Valorisation des déchets dans les fours de cimenterie. In Proceedings of the 7éme Édition COFRET, Paris, France, 23–25 April 2014; pp. 905–918.
21. Mungyeko Bisulandu, B.-J.R.; Marias, F. Modeling of the Thermochemical Conversion of Biomass in Cement Rotary Kiln. *Waste Biomass Valor.* **2021**, *12*, 1005–1024. [CrossRef]
22. Mujumdar, K.S.; Ranade, V.V. Simulation of Rotary Cement Kilns Using a One-Dimensional Model. *Chem. Eng. Res. Des.* **2006**, *84*, 165–177. [CrossRef]
23. Mujumdar, K.S.; Arora, A.; Ranade, V.V. Modeling of Rotary Cement Kilns: Applications to Reduction in Energy Consumption. *Ind. Eng. Chem. Res.* **2006**, *45*, 2315–2330. [CrossRef]
24. Darabi, P. A Mathematical Model for Cement Kilns. Master's Thesis, University of British Columbia, Vancouver, BC, Canada, 2007. [CrossRef]
25. Colina-Morles, E.; Medina, J.; Falconí, M.; Morocho, V. Phenomenological modelling and computer simulation of a clinker kiln. In *Proceedings of the 2016 IEEE Ecuador Technical Chapters Meeting (ETCM), Guayaquil, Ecuador, 12–14 October 2016*; IEEE: Piscataway, NJ, USA, 2016.
26. González, H.; Zarate Evers, C.M.; Alviso, D.; Rolon, J.C. Numerical study of a rotary kiln. A case study of an industrial plant in Paraguay. In Proceedings of the 16th Brazilian Congress of Thermal Sciences and Engineering, Vitória, Brazil, 7–10 November 2016. [CrossRef]

27. Abdulkadir, A.A.A. Modeling of Solid Reaction Behavior in Direct Heated Rotary Kilns. Ph.D. Thesis, Otto-von-Guericke-University of Magdeburg, Magdeburg, Germany, 2017.
28. Pieper, C.; Liedmann, B.; Wirtz, S.; Scherer, V.; Bodendiek, N.; Schaefer, S. Interaction of the combustion of refuse derived fuel with the clinker bed in rotary cement kilns: A numerical study. *Fuel* **2020**, *266*, 117048. [CrossRef]
29. Martin, G. Chemical Engineering and Thermodynamics applied to the Cement Rotary Kiln. *Nature* **1932**, *130*, 867. [CrossRef]
30. Georgallis, M. Mathematical Modelling of Lime Kilns. Ph.D. Thesis, University of British Columbia, Vancouver, BC, Canada, 2004. [CrossRef]
31. Csernyei, C.; Straatman, A.G. Numerical modeling of a rotary cement kiln with improvements to shell cooling. *Int. J. Heat Mass Transf.* **2016**, *102*, 610–621. [CrossRef]
32. Perry, R.H.; Green, D.W. (Eds.) *Perry's Chemical Engineers' Handbook*, 8th ed.; McGraw-Hill: New York, NY, USA, 2008.
33. Haas, J.L., Jr.; Robinson, G.R., Jr.; Hemingway, B.S. Thermodynamic tabulations for selected phases in the system CaO-Al_2O_3-SiO_2-H_2 at 101.325 kPa (1 atm) between 273.15 and 1800 K. *J. Phys. Chem. Ref. Data* **1981**, *10*, 575–670. [CrossRef]
34. Mai, N.L.; Hoang, N.-H.; Do, H.T.; Pilz, M.; Trinh, T.T. Elastic and thermodynamic properties of the major clinker phases of Portland cement: Insights from first principles calculations. *Constr. Build. Mater.* **2021**, *287*, 122873. [CrossRef]
35. Kurth, S.; Marques, M.A.L.; Gross, E.K.U. Density-Functional Theory. In *Encyclopedia of Condensed Matter Physics*; Elsevier: Amsterdam, The Netherlands, 2005; pp. 395–402. [CrossRef]
36. Smith, N.O. The difference between C_p and C_v for liquids and solids. *J. Chem. Educ.* **1965**, *42*, 654. [CrossRef]
37. Mastorakos, E.; Massias, A.; Tsakiroglou, C.D.; Goussis, D.A.; Burganos, V.N.; Payatakes, A.C. CFD predictions for cement kilns including flame modelling, heat transfer and clinker chemistry. *Appl. Math. Model.* **1999**, *23*, 55–76. [CrossRef]
38. Abdolhosseini Qomi, M.J.; Ulm, F.-J.; Pellenq, R.J.-M. Physical Origins of Thermal Properties of Cement Paste. *Phys. Rev. Appl.* **2015**, *3*, 064010. [CrossRef]
39. Spang, H.A. A dynamic model of a cement kiln. *Automatica* **1972**, *8*, 309–323. [CrossRef]

Disclaimer/Publisher's Note: The statements, opinions and data contained in all publications are solely those of the individual author(s) and contributor(s) and not of MDPI and/or the editor(s). MDPI and/or the editor(s) disclaim responsibility for any injury to people or property resulting from any ideas, methods, instructions or products referred to in the content.

https://doi.org/10.3390/physchem6010010